Identifying modal properties of trees with Bayesian inference

Daniel C. Burcham*[a,b], Siu-Kui Au[c]

*Corresponding author

[a] Center for Urban Greenery and Ecology, National Parks Board, 259569 Singapore

[b] Department of Horticulture and Landscape Architecture, Colorado State University, Fort Collins, CO 80523

[c] School of Civil and Environmental Engineering, Nanyang Technological University, 639798 Singapore

Abstract

In forested landscapes, the presence of trees enhances turbulent airflow governing the exchange of momentum, heat, and gas between the atmosphere and biosphere, especially when horizontal motion dominates near-surface winds, and tree vibration is a prominent feature of the dynamic interaction between wind and trees. The vibration characteristics of trees reflect their underlying mechanical properties (i.e., mass, stiffness, damping) and govern their response to dynamic loads. Despite numerous investigations of tree vibration, there have been few studies examining methodological improvements for identifying and characterizing variability in the modal properties of trees during ambient wind excitation. In the engineering disciplines, however, there are several techniques commonly used to estimate the modal properties of a structure from its ambient vibration, often called 'operational modal analysis' (OMA). Operating in the frequency domain, this study examined the use of Bayesian OMA for identifying several important modal properties, including frequencies, damping ratios, and partial mode shapes, as well as their identification uncertainty. Using the ambient vibration recorded on a mature *Hopea odorata* Roxb. (Dipterocarpaceae) tree over a one-week period, the identified modal properties and associated uncertainties were physically reasonable and consistent with previous

measurements for trees, and the identification uncertainty was much greater for damping ratio than frequency, which can be explained theoretically. Beyond the consistency with existing measurements, the analysis also yielded new insight about the vibration behavior of large trees. The modal properties varied considerably over consecutive one-hour intervals, and the changes were likely related to differences in wind excitation during each period, suggesting the existence of amplitude dependence in the modal properties of trees. Over the same periods, there were consistently two close modes (i.e., with similar frequencies), oriented approximately orthogonal to one another, near the tree's fundamental frequency. With additional evaluation and refinement, the techniques can be used for OMA of trees in different settings.

Highlights

- Using Bayesian inference, the modal properties of trees were estimated from ambient vibrations
- The identification uncertainty of modal properties was quantified and explained theoretically
- Frequencies and damping ratios were physically reasonable and agree with existing measurements
- The measurements revealed new features of the vibration behavior of trees over a range of conditions

Keywords:

Ambient modal identification, BAYOMA, Biomechanics, Operational modal analysis, Tree sway

1 Introduction

Under ambient conditions, trees predominantly dissipate momentum intercepted from the moving wind by swaying (i.e., vibrating) at a fundamental mode involving trunk bending (Schindler et al., 2013a, 2010). Since a tree's vibration characteristics govern its response to dynamic wind loads, many researchers have investigated the vibration properties of trees in various settings (de Langre, 2019), often seeking an improved understanding of wind damage to trees (Moore and Maguire, 2004). For a given species, the fundamental mode frequency varies inversely proportional to tree size in the decihertz range (Jackson et al., 2019). Despite concerns about the possibility of resonant amplification from wind loads acting near a tree's fundamental mode (Mayer, 1987), several studies have demonstrated that wind excitation and tree vibration primarily occur at distinct, separate frequencies (Gardiner, 1995; Scannell, 1983; Schindler and Mohr, 2018), and this may allow trees to efficiently dissipate kinetic energy by swaying without the harmful dynamic effects of wind loads primarily acting at frequencies below their natural frequency (Schindler and Mohr, 2019). Apart from the mechanical stability of trees, other studies have suggested that tree vibration affects important physiological processes, including photosynthetic rates (Burgess et al., 2016) and gas exchange with the surrounding environment (Roden and Pearcy, 1993).

Many researchers have used free vibration tests to examine variability in vibration properties associated with tree size (Bruchert and Gardiner, 2006; Jonsson et al., 2007), leaf condition (Baker, 1997; Miesbauer et al., 2014), and crown architecture (Kane et al., 2014; Sellier and Fourcaud, 2005). Although Scannell (1983) reported broad agreement between the natural frequency during free and wind-induced vibration of Sitka spruce [*Picea*

sitchensis (Bong.) Carr. (Pinaceae)], there is some evidence that wind loads mediate the activation of vibratory modes in trees (Schindler et al., 2013b, 2010), and it is useful to examine modal properties in the context of a specific loading environment (Schindler and Mohr, 2018). Due to viscous damping (Jonsson et al., 2007), the different methods used to deflect trees for free vibration testing may affect damping ratio estimates (Kane, 2018; Reiland et al., 2015), preventing straightforward comparisons between existing measurements. Moreover, the point loads applied to the trunk during free vibration testing poorly approximate distributed wind loads acting primarily on leaves (Vogel, 2009), and it can be practically challenging to deflect trees for free vibration testing with a heavy-duty rigging system, especially for large trees.

Alternatively, many researchers have examined tree vibration during ambient wind excitation, often involving measurements recorded over extended time periods (Bunce et al., 2019; Granucci et al., 2013; Schindler et al., 2013b). Most studies estimated modal frequencies, especially for the fundamental mode, from these measurements (Schindler et al., 2012; van Emmerik et al., 2018). Despite many studies of damping mechanisms in trees (Spatz and Theckes, 2013), there are no available reports of damping ratios during ambient wind excitation, since researchers have exclusively used free vibration (Gardiner, 1989; Milne, 1991) and, occasionally, forced vibration (Castro-Garcia et al., 2008) tests to estimate damping ratios for trees. Although many acknowledge the possibility of using ambient vibration measurements to monitor changes in a tree's physical condition (Ciruzzi and Loheide, 2019; Gougherty et al., 2018; van Emmerik et al., 2017), the variation in vibration properties associated with tree condition over time may be obscured by other sources of variability (Kooreman, 2013). There is a need for rigorous measurement and analysis

97 techniques to estimate the modal properties of trees from ambient vibration, and, if
98 possible, quantify their identification uncertainty.
99
100 Frequently encountered in the engineering disciplines, the attempt to identify modal
101 properties from ambient vibration data, without knowing the excitation, is often called
102 ambient modal identification or 'operational modal analysis' (OMA). Many different
103 methods have been developed for the analysis of structural vibrations from ambient
104 measurements. For example, stochastic subspace identification (SSI) (Peeters and De Roeck,
105 2001; van Overschee and de Moor, 1996) estimates modal properties based on the state
106 matrices of a time-invariant state-space model estimated by regression. Frequency domain
107 decomposition (FDD) (Brincker et al., 2001; Pintelon and Schoukens, 2001) decomposes the
108 power spectral density matrix estimated from measured data and uses the resulting
109 eigenvectors and eigenvalues to estimate the mode shapes and modal properties,
110 respectively. See Au (2017), Brincker and Ventura (2015), and Schipfors and Fabbrocino
111 (2014) for more detailed summaries of OMA. While these methods can be viewed as
112 constructing a statistical estimator to approximate the modal parameters sought from the
113 measured data, Bayesian methods consider the modal parameters as random variables
114 whose joint probability distribution depends on available information contained in the data,
115 as well as modeling assumptions. Among different Bayesian formulations, the methods
116 employing the fast Fourier transform (FFT) of ambient vibration time histories in a
117 frequency band near target modes can be reasonably configured, by adjusting the size of
118 the frequency band used for analysis, to estimate the most probable values and associated
119 uncertainties of modal properties (Au, 2017; Yuen and Katafygiotis, 2003), and there have
120 been many recent improvements to the associated theory, algorithmic efficiency (Zhu et al.,

2021), and management of identification uncertainty for different test configurations (Au et al., 2021).

Despite the potential convenience and suitability of OMA for characterizing vibration of structures experiencing environmental loads, the techniques have mostly been used on buildings, bridges, and other manmade structures (Ameri et al., 2013; DeVivo et al., 2013). See Brownjohn et al. (2011) for a review of vibration monitoring of civil infrastructure. However, there are important differences between the dynamic mechanical behavior of trees and manmade structures. In unsteady flows, leaves, easily accelerated because of their low virtual mass (Daniel, 1984), contribute most of the total drag acting on a tree (Vollsinger et al., 2005), but the slender, flexible branches to which they are attached create a slowed, large deformation response to applied loads with adaptive reconfiguration that minimizes total drag (Vogel, 2009). In general, the damping ratios of trees are greater than most manmade structures, and the vibration properties of trees change over time with meteorological seasons (Granucci et al., 2013; Reiland et al., 2015) and life stages (Sellier and Suzuki, 2020). To facilitate the use and examine the suitability of similar techniques for studying the dynamic mechanical behavior of trees, the objective of this study was to introduce and apply Bayesian OMA to estimate the modal properties of trees. For this purpose, an overview of the methodology is given in Section 2, covering basic assumptions, formulation, and computational aspects. In addition to the estimate itself, the identification uncertainty can be computed (Section 2.4) to inform the quality of the estimate, and the identification uncertainty expected for various test configurations can be evaluated with simple formulas during the planning stage of investigations (Section 2.5). In Section 3, the method is used to study the modal properties of a tree with short-term (Section 3.3) and

145 long-term monitoring data (Section 3.4), distinguishing between observations arising from
146 identification uncertainty and variability due to actual changes in the tree or its
147 environment. In Section 4, the method is appraised for the particular application, and the
148 need for additional work is outlined, especially to optimize the techniques for use on trees.
149 For reference, a summary of abbreviations and symbols used in this work can be found in
150 Appendix I.
151

152 **2 Bayesian Inference using ambient vibration data**

153 An overview of Bayesian modal identification using ambient vibration data is presented in
154 this section, and the following summary provides a conceptual overview of the key formulas
155 and their role in the analysis procedure:
156 Based on the outlined theory and assumptions (Section 2.1), the theoretical expression for
157 the FFT of ambient vibration data in equation (2) contributes to the derivation of the
158 corresponding power spectral density (PSD) matrix in equation (5). Based on this expression
159 for the PSD matrix, the most probable value (MPV) of the modal parameters can be
160 obtained through iterative optimization by minimizing the negative log-likelihood function
161 (NLLF) in equation (8). The remaining uncertainty about the parameters, encapsulated in
162 their posterior covariance matrix, can be determined by evaluating the Hessian of the NLLF
163 at the MPV and inverting the resulting matrix; see Au (2017) for more detailed information
164 about each step of the analysis process. The development and presentation of formulas
165 throughout this work assumed the use of translational acceleration measurements of
166 ambient vibration, but the outlined method is suitable for a general response (e.g.,
167 translational or angular motion recorded as displacement, velocity, or acceleration). A

numerical implementation of the method, available upon request, was developed using MATLAB R2020a (The MathWorks, Inc., Natick, MA).

2.1 Context and assumptions

Let $\{\ddot{\boldsymbol{x}}_j\}_{j=0}^{N-1}$, with each $\ddot{\boldsymbol{x}}_j$ being a $n \times 1$ vector, denote the ambient acceleration response of a structure at n measured degrees of freedom (DOFs) and sampled at time interval Δt (s) with N sampled points per DOF. The number of measured DOFs n is generally different from (and is typically much smaller than) the total number of DOFs governing the dynamics of the structure. The latter can be possibly infinite, but it is otherwise irrelevant to the theory in this work that focuses on modal identification rather than predicting the time-varying structural response. For clarity, the variable n exclusively refers to the measured DOFs throughout this work (Appendix I). The scaled FFT of $\{\ddot{\boldsymbol{x}}_j\}$ at frequency $\mathrm{f}_k = k/N\Delta t$ (Hz) is defined as:

$$\boldsymbol{F}_k = \sqrt{\frac{2\Delta t}{N}} \sum_{j=0}^{N-1} \ddot{\boldsymbol{x}}_j e^{-2\pi \boldsymbol{i} jk/N}, \quad (1)$$

where $\boldsymbol{F}_k$ is a $n \times 1$ complex valued vector. The sequence $\{\boldsymbol{F}_k\}_{k=0}^{N-1}$ can be obtained efficiently using the standard FFT algorithm (Cooley and Tukey, 1965) from the sequence $\{\ddot{\boldsymbol{x}}_j\}_{j=0}^{N-1}$. The scaling factor $\sqrt{2\Delta t/N}$ ensures that the variance of each component of $\boldsymbol{F}_k$ gives the corresponding one-sided power spectral density (PSD). Unless otherwise stated, the sequence $\{\boldsymbol{F}_k\}_{k=0}^{N-1}$ in equation (1) will be simply referred to as the FFT of $\{\ddot{\boldsymbol{x}}_j\}_{j=0}^{N-1}$.

Operating in the frequency domain, the FFT values are used as the input data for identifying modal properties. Although the FFT values are often averaged when plotting the power

spectrum for visualizing modes (Section 2.6), the values are not averaged in equation (1) for Bayesian modal identification. Instead of using the whole sequence $\{\boldsymbol{F}_k\}_{k=0}^{N-1}$, however, only the FFT values in a selected frequency band near the modes of interest are used. The frequency band can be selected using the singular value (SV) spectrum (Section 2.6). Rather than using the entire sequence $\{\boldsymbol{F}_k\}_{k=0}^{N-1}$ from zero to the Nyquist frequency, the modeling of modal dynamics (equation (5)) and computations used to identify modal properties (Section 2.3) are significantly simplified by only considering the modes near the natural frequencies of interest. The FFT values in other, excluded frequency bands are not considered, making the modal identification process immune to activities (i.e., FFT values) in those bands that are either irrelevant to the subject modes or difficult to model.

Modal dynamics under stochastic loads

The following section provides a summary of the conventional assumptions used to model structural dynamics, including the definition of several properties related to those identified from ambient vibration data. For a tree modeled as a structure with displacement response vector $\boldsymbol{X}(t)$ containing all governing DOFs, the standard second-order differential equation can be used to model the response: $\boldsymbol{M}\ddot{\boldsymbol{X}}(t) + \boldsymbol{C}\dot{\boldsymbol{X}}(t) + \boldsymbol{K}\boldsymbol{X}(t) = \boldsymbol{F}(t)$, where $\boldsymbol{M}$, $\boldsymbol{C}$, and $\boldsymbol{K}$ are the (constant) mass matrix, damping matrix, stiffness matrix, respectively, and $\boldsymbol{F}(t)$ is the force vector. For each mode i, the (undamped) natural frequency, ω_i (rad s^{-1}), and (full) mode shape, $\boldsymbol{\psi}_i$ (a dimensionless column vector with a number of entries corresponding to the total DOFs), are defined by the eigenvalue equation $\boldsymbol{K}\boldsymbol{\psi}_i = \omega_i^2\boldsymbol{M}\boldsymbol{\psi}_i$. Assuming 'classical damping', i.e., $\boldsymbol{\psi}_i^T\boldsymbol{M}\boldsymbol{\psi}_j = \boldsymbol{\psi}_i^T\boldsymbol{K}\boldsymbol{\psi}_j = 0$ whenever $i \neq j$, the response is given by a superposition of modes, i.e., $\boldsymbol{X}(t) = \sum \boldsymbol{\psi}_i\,\eta_i(t)$, summed over all the modes and where $\eta_i(t)$ is the (scalar) ith modal response. Mathematically, a structure is classically damped if

214 and only if $\boldsymbol{KM^{-1}C} = \boldsymbol{CM^{-1}K}$ (Caughey and O'Kelly, 1965). However, this condition can
215 only be examined in theoretical situations amenable to such mathematical treatment, and
216 the mechanisms responsible for damping in many structures are often more complex (e.g.,
217 hysteretic and amplitude dependent) than viscous damping. Still, many authors have shown
218 that the damping mechanisms are often well approximated by a viscous model (Jeary,
219 1997), even for trees (Jonsson et al., 2007). Consistent with the conventional theoretical
220 analysis of structural dynamics, the (uncoupled) modal equation $\ddot{\eta}_i(t) + 2\zeta_i\omega_i\dot{\eta}_i(t) +$
221 $\omega_i^2\eta_i(t) = p_i(t)$, where $\zeta_i = (\boldsymbol{\psi}_i^T\boldsymbol{C}\boldsymbol{\psi}_i)/2\omega_i(\boldsymbol{\psi}_i^T\boldsymbol{M}\boldsymbol{\psi}_i)$ is the (dimensionless) damping ratio
222 and $p_i(t) = \boldsymbol{\psi}_i^T\boldsymbol{F}(t)/(\boldsymbol{\psi}_i^T\boldsymbol{M}\boldsymbol{\psi}_i)$ is the modal force (per unit modal mass) can be obtained by
223 substituting $\boldsymbol{X}(t) = \sum \boldsymbol{\psi}_i\eta_i(t)$ into the equation of motion $\boldsymbol{M}\ddot{\boldsymbol{X}}(t) + \boldsymbol{C}\dot{\boldsymbol{X}}(t) + \boldsymbol{K}\boldsymbol{X}(t) =$
224 $\boldsymbol{F}(t)$ and assuming classical damping. During ambient modal identification, however, the
225 modal properties are estimated using only ambient vibration data at a limited number of
226 DOFs, instead of relying on the preceding theoretical relationships. Using ambient vibration
227 data, for example, it is possible to estimate ζ_i and the PSD of $p_i(t)$, but it is often not
228 possible to determine $\boldsymbol{C}$ or the PSD of $\boldsymbol{F}(t)$, due to a lack of information about the complete
229 structural response and excitation force.
230
231 **PSD of ambient vibration data**
232 Confining the response of a tree to the DOFs measured during vibration monitoring, i.e.,
233 $\boldsymbol{x}(t)$ contains selected entries of $\boldsymbol{X}(t)$ at the measured DOFS, modal superposition becomes
234 $\boldsymbol{x}(t) = \sum \boldsymbol{\varphi}_i\eta_i(t)$, where $\boldsymbol{\varphi}_i$ is the ith mode shape ($n \times 1$ vector) confined to the measured
235 DOFs, often distinguished from the 'full' mode shape $\boldsymbol{\psi_i}$, containing all governing DOFs, as
236 the 'partial' mode shape. Assuming the measured ambient acceleration data comprises the
237 modal response and noise, $\boldsymbol{\varepsilon}$, i.e., $\ddot{\boldsymbol{x}}_j = \sum \boldsymbol{\varphi}_i\ddot{\eta}_i(t_j) + \boldsymbol{\varepsilon}(t_j)$ where $t_j = j\Delta t$, and m modes

exist in the selected frequency band, limiting the range of k considered (equation (1)), the (scaled) FFT of this relationship becomes:

$$\boldsymbol{F}_k = \sum_{i=1}^{m} \boldsymbol{\varphi}_i h_{ik} p_{ik} + \boldsymbol{\varepsilon}_k, \quad (2)$$

where $\boldsymbol{\varepsilon}_k$ $(n \times 1)$ is the FFT of data noise, p_{ik} is the FFT of modal force p_i, and

$$h_{ik} = \frac{1}{1-\beta_{ik}^2-2\zeta_i\beta_{ik}\boldsymbol{i}} \quad (3)$$

is the (dimensionless) frequency response function between p_i and $\ddot{\eta}_i$, where

$$\beta_{ik} = \frac{f_i}{\mathrm{f}_k} \quad (4)$$

is the frequency ratio of the modal frequency f_i to the FFT frequency f_k, the reciprocal of the same equation often used for displacement. In equation (2), the term $h_{ik}p_{ik}$, equal to the FFT of $\ddot{\eta}_i$, can be derived by taking the Fourier transform (FT) of the modal equation $\ddot{\eta}_i(t) + 2\zeta_i\omega_i\dot{\eta}_i(t) + \omega_i^2\eta_i(t) = p_i(t)$ and substituting the FT of $\dot{\eta}_i(t)$ and $\eta_i(t)$ with the FT of $\ddot{\eta}_i(t)$ divided by $\boldsymbol{i}\omega_k$ and $(\boldsymbol{i}\omega_k)^2$, respectively.

Under ambient vibration, the modal forces are assumed to be a stationary stochastic process. Practically, this assumption requires that the statistics of the modal forces (e.g., mean, variance, correlation) remain constant within the analyzed segment of ambient vibration data (Section 3.4). The instrument noise of each data channel is assumed to be independent and identically distributed, often reasonable for data obtained from the same hardware environment, and the noise is also assumed to be unaffected by modal forces. Based on these assumptions, the $n \times n$ PSD matrix of ambient vibration data is given by:

$$\boldsymbol{E}_k = E[\boldsymbol{F}_k\boldsymbol{F}_k^*] = \sum_{i,j=1}^{m} \boldsymbol{\varphi}_i\boldsymbol{\varphi}_j^T h_{ik}h_{jk}^* S_{ij} + S_e\boldsymbol{I}_n, \quad (5)$$

where $\boldsymbol{I}_n$ denotes the $n \times n$ identity matrix, S_e is the PSD of noise, and $S_{ij} = E\left[p_{ik}p_{jk}^*\right]$ is the cross-PSD between the modal forces of mode i and j. In the middle expression of

equation (5), $E[\cdot]$ denotes the expectation of the argument quantity. Often justified because the bandwidth is small (i.e., on the order of ζ_i), both S_e and S_{ij} are assumed to be constant within the selected band. The theory and methodology presented in this work use acceleration measurements, but they are generally applicable for other types of measurements, e.g., velocity and displacement, provided that the frequency response function in equation (3) is modified accordingly. As outlined at the beginning of Section 2, the theoretical expression for the PSD matrix in equation (5) was derived from the scaled FFT of the acceleration data modeled in equation (2), but the expression of $\boldsymbol{F}_k$ in equation (2) will not be directly used to estimate modal properties. Instead, the modal properties can be identified from the collection of $\boldsymbol{F_k}$ in a selected frequency band, but the identification process requires additional computations, outlined in the following section.

2.2 Bayesian formulation

Let $\boldsymbol{\theta}$ be a vector consisting of the modal parameters to be identified from the FFT $\{\boldsymbol{F}_k\}$ within the selected frequency band. In a Bayesian perspective, $\boldsymbol{\theta}$ is modeled as a random vector whose probability distribution depends on available information. The information that the data $\{\boldsymbol{F}_k\}$ provides about $\boldsymbol{\theta}$ is encapsulated in the posterior distribution $p(\boldsymbol{\theta}|\{\boldsymbol{F}_k\})$, which is conditional on $\{\boldsymbol{F}_k\}$. Using Bayes' theorem, this can be expressed as:

$$p(\boldsymbol{\theta}|\{\boldsymbol{F}_k\}) = p(\{\boldsymbol{F}_k\}|\boldsymbol{\theta})\,\frac{p(\boldsymbol{\theta})}{p(\{\boldsymbol{F}_k\})}. \quad (6)$$

Viewed as a distribution and, hence, a function of $\boldsymbol{\theta}$, the term $p(\{\boldsymbol{F}_k\})$ does not vary with respect to $\boldsymbol{\theta}$. Mathematically, $p(\{\boldsymbol{F}_k\})$ is equal to the integral of $p(\{\boldsymbol{F}_k\}|\boldsymbol{\theta})p(\boldsymbol{\theta})$ over all values of $\boldsymbol{\theta}$; it is a normalizing constant ensuring $p(\boldsymbol{\theta}|\{\boldsymbol{F}_k\})$ integrates to one, consistent with the basic properties of a probability density function. Often called the 'prior

distribution,' the term $p(\boldsymbol{\theta})$ reflects the state of knowledge about $\boldsymbol{\theta}$ before data is available. The term $p(\{\boldsymbol{F}_k\}|\boldsymbol{\theta})$, called the 'likelihood function,' is the most important term that must be derived based on modelling assumptions to identify the parameters ($\boldsymbol{\theta}$) sought from measured data ($\{\boldsymbol{F}_k\}$). In modal identification problems with hundreds of FFT values in a frequency band, the prior distribution varies slowly with $\boldsymbol{\theta}$ compared to the likelihood function $p(\{\boldsymbol{F}_k\}|\boldsymbol{\theta})$, and it can be practically treated as invariant with respect to $\boldsymbol{\theta}$. In practice, vibration monitoring often yields data with a sufficiently large number of FFT values in a frequency band. Since $p(\{\boldsymbol{F}_k\})$ and $p(\boldsymbol{\theta})$ do not vary with respect to $\boldsymbol{\theta}$ in such circumstances, the posterior distribution is directly proportional to the likelihood function. For sufficiently long stationary data, it can be shown that the FFT $\{\boldsymbol{F}_k\}$ at different frequencies are independent, and each follows a complex Gaussian distribution with auto-covariance matrix equal to $\boldsymbol{E}_k$ (Brillinger, 2001). Therefore, the posterior distribution can be written as:

$$p(\boldsymbol{\theta}|\{\boldsymbol{F}_k\}) \propto p(\{\boldsymbol{F}_k\}|\boldsymbol{\theta}) = e^{-L(\{\boldsymbol{F}_k\},\boldsymbol{\theta})}, \tag{7}$$

where

$$L(\{\boldsymbol{F}_k\},\boldsymbol{\theta}) = nN_f ln\pi + \sum_k \ln|\boldsymbol{E}_k| + \sum_k \boldsymbol{F}_k^* \boldsymbol{E}_k^{-1} \boldsymbol{F}_k \tag{8}$$

is the negative log-likelihood function (NLLF), often used in analysis and computation; N_f is the number of FFT points in the selected frequency band. Equation (7) with $L(\{\boldsymbol{F}_k\},\boldsymbol{\theta})$ was derived directly from the standard formula for the joint complex Gaussian probability density function of independent vectors $\{\boldsymbol{F}_k\}$, each with covariance matrix $\boldsymbol{E}_k$ (Brillinger, 2001). Since the NLLF and, hence, the posterior distribution depend on $\boldsymbol{\theta}$ entirely through $\boldsymbol{E}_k$, it is apparent that the modal parameters in the problem comprise those necessary to specify $\boldsymbol{E}_k$, i.e.,

$$\boldsymbol{\theta} = \{f_i, \zeta_i, \boldsymbol{\varphi}_i, S_{ij}, S_e : i, j = 1, \dots m\} \quad (9)$$

where S_{ij} is the complex conjugate of S_{ji} ($S_{ij} = \overline{S_{ji}}$). On the other hand, the mode shapes are subjected to a scaling constraint, often normalized to have unit norm, i.e., each $n \times 1$ vector $\boldsymbol{\varphi}_i$ has a sum of squares equal to 1. The symbolic expression in equation (9) is treated, conceptually and computationally (Section 2.3), as a vector containing all the modal properties.

2.3 Posterior statistics computation

As is common in Bayesian inference problems, the posterior distribution of $\boldsymbol{\theta}$ does not correspond to any standard distribution because the likelihood function $L(\{\boldsymbol{F}_k\}, \boldsymbol{\theta})$ depends on $\boldsymbol{\theta}$ in a nonlinear manner unsuitable for analytical treatment mathematically. Nevertheless, the distribution of $\boldsymbol{\theta}$ is often unimodal in typical modal identification applications with hundreds of FFT values in a frequency band, and a Gaussian distribution provides a good approximation of the empirical distribution of $\boldsymbol{\theta}$. Consequently, the (Gaussian) posterior distribution is characterized by the mean vector and covariance matrix of $\boldsymbol{\theta}$. Analogous to the best estimate in non-Bayesian methods, the mean is a $p \times 1$ vector ($p =$ number of parameters) that contains the most probable value (MPV) of $\boldsymbol{\theta}$. The covariance matrix is a $p \times p$ symmetric matrix that can be used to quantify the remaining identification uncertainty about $\boldsymbol{\theta}$ despite the use of data.

Mathematically, it can be shown that the MPV minimizes the NLLF, and the posterior covariance matrix is equal to the inverse of the Hessian matrix of the NLLF at the MPV. Due to the large number of parameters in $\boldsymbol{\theta}$ and its nonlinear appearance in the NLLF, it is not possible to obtain an analytical solution for the MPV, and it can be computationally

prohibitive to use generic optimization algorithms (e.g., simplex search, Newton-Rapson method) that do not require information about the functional relationship between variables. Instead, iterative algorithms that exploit the special mathematical (matrix algebra) structure of the NLLF in different cases have been developed to estimate the MPV, especially for well-separated modes ($m = 1$) (Au, 2011) and general multiple (possibly 'close', i.e., with similar frequencies) modes ($m > 2$) (Au, 2012; Li and Au, 2019). In contrast, analytical formulas have been developed for computing the Hessian of the NLLF (Au, 2012, 2011; Li and Au, 2019). Using the numerical algorithms, the estimates for well-separated modes can be obtained in a matter of seconds, but the time required to compute estimates for close modes is often significantly longer, depending on the number of modes, proximity of modes, and signal noise. For two close modes, the estimation time typically ranges from a few seconds to a few minutes. In some cases, a solution may not be obtained if the convergence criteria of the iterative algorithm are not satisfied. However, the failure to converge usually indicates that information in the data is insufficient to identify the parameters, and the estimates given by other explicit methods lacking convergence issues will likely be poor or misleading.

2.4 Quantification of identification uncertainty

For scalar parameters, such as the natural frequency and damping ratio, the identification uncertainty can be quantified in a dimensionless manner by the 'coefficient of variation' (c.o.v.), defined as the ratio of the standard deviation of a parameter to the corresponding MPV. The former is the square root of variance, which is the corresponding diagonal entry of the posterior covariance matrix. Based on experience, a c.o.v. near 10% and 30% often suggest low and moderate uncertainty, respectively. Otherwise, a higher c.o.v. usually

355 indicates a poor estimate, possibly arising from, in the context of the model used, a lack of
356 sufficient evidence in the data about the parameter or a violation of modeling assumptions.
357
358 Since the identified (partial) mode shape, $\boldsymbol{\varphi}_i$, is a $n \times 1$ vector subjected to scaling
359 constraint, its uncertainty quantification requires special treatment. It is not possible to
360 obtain a proper estimate of uncertainty by simply dividing the standard deviation of a
361 particular element of the mode shape vector by the MPV. Fortunately, it turns out that the
362 square root sum of the eigenvalues of the $n \times n$ covariance matrix of mode shape gives a
363 measure analogous to the c.o.v. of a scalar parameter (Au, 2017; Au and Zhang, 2011).
364

365 **2.5 Anticipating and managing identification uncertainty**

366 Based on the outlined Bayesian formulation (Section 2.2) and computational algorithms
367 (Section 2.3), the identification uncertainty of a given parameter can be calculated using
368 available data, but the estimates do not yield any a priori insight about the relationship
369 between identification uncertainty and test configurations, such as the duration of
370 measurement, sensor characteristics, and measurement positions. Recently, several
371 analytical expressions were developed that explicitly relate the posterior c.o.v. to
372 fundamental parameters (e.g., N_c, κ, γ; defined shortly) that characterize the test
373 configuration (Au et al., 2021, 2018). For example, a well-separated mode with frequency f
374 and damping ratio ζ may be identified using FFT values in the band $f(1 \pm \kappa\zeta)$, where κ is a
375 dimensionless bandwidth factor that quantifies the amount of relevant information in the
376 data. The value of κ depends on the measured data and subject mode, but a value of 5 to 10
377 is common and may be assumed in applications. The c.o.v. of frequency (δ_f) and damping
378 ratio (δ_ζ) can be anticipated using (Au, 2017; Au et al., 2018):

$$\delta_f^2 = \frac{\zeta}{2\pi N_c B_f}\left(1+\frac{a_f}{\gamma}\right) \text{ and } \delta_\zeta^2 = \frac{1}{2\pi\zeta N_c B_\zeta}\left(1+\frac{a_\zeta}{\gamma}\right), \quad (10)$$

where $N_c = (\text{data duration})/(\text{natural period})$ is a dimensionless measure of data duration, B_f and B_ζ are dimensionless 'data length factors', i.e., monotonic increasing functions (from 0 to 1) of κ that quantify the effect of κ on the effective data length:

$$B_f = \frac{2}{\pi}\left(\tan^{-1}\kappa - \frac{\kappa}{\kappa^2+1}\right) \text{ and } B_\zeta = \frac{2}{\pi}\left[\tan^{-1}\kappa + \frac{\kappa}{\kappa^2+1} - \frac{2\left(\tan^{-1}\kappa\right)^2}{\kappa}\right]; \quad (11)$$

$\gamma = S_{ii}/4S_e\zeta^2$ is the modal signal-to-noise ratio (s/n) that measures the quality of data; and a_f and a_ζ are dimensionless monotonic increasing functions of κ (Au, 2017; Au et al., 2018). Expressions with a similar mathematical form were recently developed for estimating the identification uncertainty for close modes (Au et al., 2021).

The formulas in equation (10) require that the data is distributed as the assumed likelihood function. They were derived assuming the existence of long time histories, small damping, and high s/n ratio. Offering a good approximation in many situations, the formulas guide expectations about identification uncertainty for different test configurations and allow for the optimal refinement of experimental plans. The formulas imply, for example, that the identification uncertainty decreases with γ to a non-zero value, even for a noiseless sensor ($\gamma \to \infty$), reflecting the lack of information about the input excitation. In ideal situations, the achievable precision limits from ambient vibration data occur when $\gamma \to \infty$ and the data length factors (i.e., B_f and B_ζ) are unity, and the corresponding equations simply become $\delta_f^2 = \zeta/2\pi N_c$ and $\delta_\zeta^2 = 1/2\pi\zeta N_c$. Generally, $\delta_f \propto \sqrt{\zeta}$ and $\delta_\zeta \propto 1/\sqrt{\zeta}$, which agrees with empirical observations that for small damping ratio the frequency is much easier to estimate than the damping ratio (Burcham et al., 2020; Kane et al., 2014), and the identification

uncertainty for f and ζ differ by an order of magnitude (Au, 2017; Brincker and Ventura, 2015).

2.6 Detecting modal frequencies from PSD and SV spectra

The algorithm requires an initial guess of the modal frequencies, and the values can be determined by visually identifying and manually selecting peaks in the PSD and SV spectra. The PSD spectrum depicts the frequency characteristics of a stochastic, stationary time history. For a time history containing N observations recorded at Δt (s) intervals, it is often estimated by averaging the squared modulus of the FFT computed from M non-overlapping, shorter segments, yielding a 'sample PSD' for the analyzed segment of the entire time history. At each frequency, the sample variance of the averaged PSD will be inversely proportional to M, but the frequency spacing will increase proportional to M, since $\Delta f = M/N\Delta t$ (Hz). The number of segments M should be carefully selected to avoid inflating either the sample variance or frequency spacing (Δf).

The PSD exhibits a distinct peak near the natural frequency of a mode, but it does not necessarily indicate the number of contributing modes in a frequency band. For example, three uniaxial sensors positioned at the same location and oriented identically would record very similar vibration measurements. The PSD of the recorded data would show similar distinct peaks near the same natural frequency of the structure, but the measurements clearly do not demonstrate the existence of three modes at the same frequency. However, the SV spectrum, depicting the eigenvalues of the real part of the sample PSD matrix at each frequency, can be used to detect the number of contributing modes in a frequency band. At each FFT frequency f_k, the (i, j) entry of the sample PSD matrix is equal to the average of

425 $F_{ik}F_{jk}^{*}$ over the M sets of FFTs, where F_{ik}denotes the FFT of measured DOF i of a segment

426 (similar notation for F_{jk}).

427

428 The number of contributing modes in a frequency band can be determined empirically by

429 the number of peaks in the SV spectrum. For a single, isolated mode i in a frequency band

430 unaffected by noise, the $n \times n$ PSD matrix, approximately equal to $S_{ii}|h_{ik}|^2\boldsymbol{\varphi}_i\boldsymbol{\varphi}_i^T$, has only

431 one non-zero eigenvalue proportional to $S_{ii}|h_{ik}|^2$, since $\boldsymbol{\varphi}_i$ is $n \times 1$, and the eigenvalue

432 varies with frequency in a manner similar to dynamic amplification $|h_{ik}|^2$. Due to the

433 presence of noise in most measurements, the remaining eigenvalues will actually be smaller

434 non-zero values reflecting the amount of noise in the data. For multiple modes, the

435 $n \times n$ PSD matrix will have a rank equal to the number of m contributing modes in the

436 frequency band, assuming the partial mode shapes are not co-linear. In such cases, the SV

437 spectrum will contain m eigenvalues varying with frequency in a similarly peaked manner,

438 and the remaining $(n - m)$ eigenvalues will depict the amount of noise in the data at each

439 frequency. See Shih et al. (1988) or Au (2017) for more information about detecting modal

440 frequencies from the SV spectrum.

441

442 **3 Field case study**

443 To illustrate the identification of modal properties, the Bayesian method presented in

444 Section 2 was used to estimate the modal properties of a large, open-grown tree using

445 ambient vibration measurements.

446

447 **3.1 Site and trees**

448 One *Hopea odorata* Roxb. (Dipterocarpaceae) tree was selected for measurement in this
449 study (Figure 1a). Situated in a residential landscape, the tree height and trunk diameter at
450 breast height (1.37 m above ground) were 27.4 m and 0.46 m, respectively. Commonly used
451 as an amenity tree in Southeast Asia, this species was selected because its excurrent
452 branching pattern produces a more consistent vibration behavior than decurrent branching
453 patterns (James et al., 2006).

454

455 **3.2 Sensor and data**

456 Tree movement was recorded using a triaxial accelerometer with integrated power supply
457 and data storage (AL100, Oregon Research Electronics, Tangent, Oregon) attached to the
458 trunk immediately below the crown (Figure 1b) at approximately 13 m above ground. See
459 van Emmerik et al. (2017) for more information about the accelerometer. Starting at 1800H
460 on 5 July 2018, the accelerometer recorded movement continuously at 10 Hz within a range
461 of ± 2 *g* (1 *g* = 9.81 $\mathrm{m\ s^{-2}}$) over a one-week period. Attached to the tree using two elastic
462 cords, the sensor was oriented visually with its x-axis parallel to the longitudinal axis of the
463 trunk (i.e., roughly vertical). The y- and z-axes of the sensor were similarly oriented
464 tangential and perpendicular, respectively, to the local bark surface. Using a right-handed
465 coordinate system, the sensor recorded positive accelerations along the x- and z-axes
466 downward and away from the trunk surface, respectively. For short-term monitoring,
467 mechanical fasteners will also maintain the orientation of vibration sensors, but the
468 production of wound periderm around fasteners may disturb the sensor orientation over
469 longer time periods. After linearly detrending the data, the acceleration measured along the
470 x-axis was relatively small compared to measurements on the other two axes (Figure 2), and

a slowly varying drift, likely attributed to sensor noise, was observed for the same measurements. The y and z channels generally displayed an oscillatory movement expected of ambient vibration. The data was clearly non-stationary over the time scale of one week with obvious fluctuations in signal variance likely associated with changes in environmental conditions. Given the assumption of a stationary response for modal identification, the entire one-week data record was divided into 165 non-overlapping one-hour segments. The modal properties of the tree were identified using each one-hour segment of data, expected to be stationary within each segment, separately (Section 3.4).

Figure 1 The ambient vibrations of one *Hopea odorata* Roxb. (Dipterocarpaceae) (a) were monitored using an accelerometer attached to the trunk immediately below the crown (b).

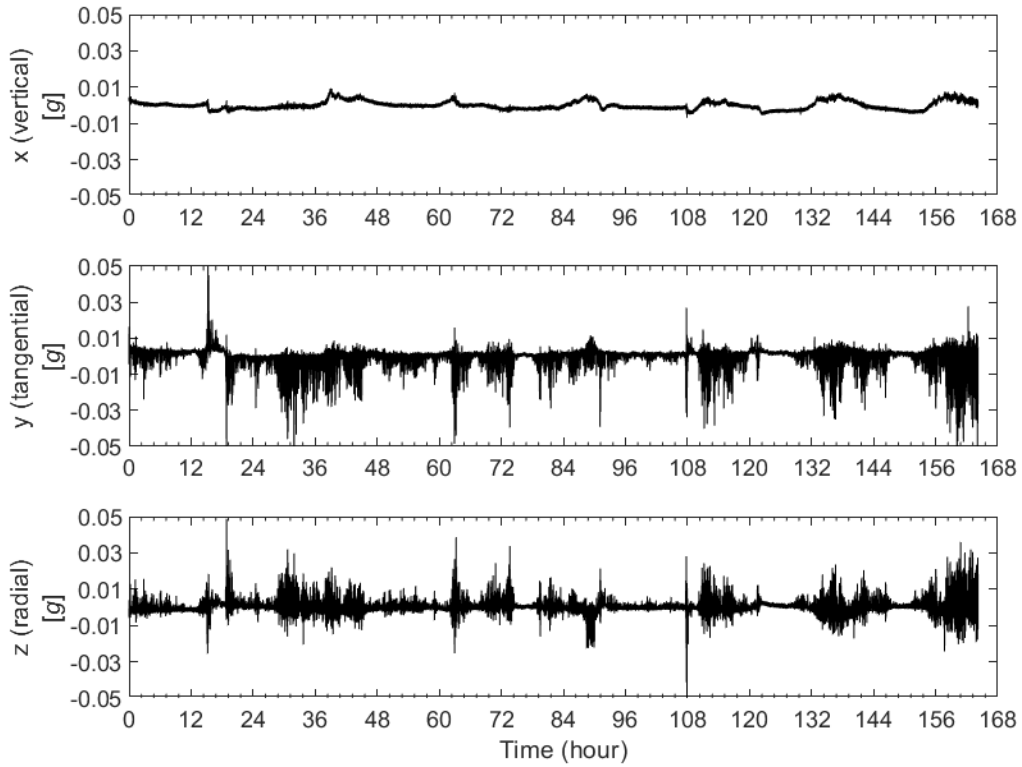

Figure 2 Time history of ambient vibration (detrended) recorded over a one-week period on a mature *Hopea odorata* Roxb. (Dipterocarpaceae) tree.

3.3 Analysis of a typical short time history

Using data from the first hour of measurements, the PSD spectrum was computed by dividing all observations into 18 non-overlapping time windows of 200 s each, and the resulting frequency spacing was 1/200 = 0.005 Hz (i.e., 200 FFT points shown in the range from 0.005 to 1 Hz). The frequency spacing is also equal to the lowest non-zero frequency displayed in the spectrum. For clarity around the lower frequencies, the limited frequency range was selected because an initial examination of the data from other time intervals showed qualitatively similar spectra with peaks in PSD at frequencies below 1 Hz. Except for the broad peaks in PSD near 0.15 Hz and 0.5 Hz, likely associated with the vibration modes of the tree, there was a slowly decreasing trend in PSD with increased frequency for all data

channels, especially around the lower frequencies (Figure 3a). Roughly inversely proportional to frequency, this spectral feature was caused by the pink noise of the sensor. Since the x channel was minimally affected by tree vibration, it roughly reflected the noise level present in the sensor at most frequencies, and the PSD for all three channels converged to similar values at frequencies above 0.7 Hz. The peak around 0.15 Hz in the x channel likely reflects the small projection of large horizontal accelerations onto the longitudinal axis. Except for very low frequencies, the noise PSD for the x channel was about $10^{-8} g^2 \text{ Hz}^{-1}$, which is typical for MEMS accelerometers.

The peaks near 0.15 Hz and 0.5 Hz (Figure 3a) were likely caused by the vibration modes of the tree. The Bayesian method in Section 2, as implemented algorithmically by Au (2012), was used to estimate modal properties for the lowest two modes near 0.15 Hz, often the subject of related investigations. As mentioned at the end of Section 2.1, the peaks in PSD associated with measurements from the x (longitudinal), y (tangential) and z (radial) channels merely indicate that the corresponding directions were affected by the mode, but this does not reveal the number of modes around this frequency. The two lines near 0.15 Hz showing peaks in the SV spectrum (Figure 3b) suggested that two close modes, i.e., with similar frequencies, occurred near the frequency.

Using the FFT of acceleration data on a frequency band covering the modes selected from the SV spectrum, the MPV of modal parameters during the first hour of ambient vibration was estimated using the Bayesian formulated iterative algorithm (Table 1). The MPVs for the natural frequencies of the two modes, at approximately 0.13 Hz (mode 1) and 0.15 Hz (mode 2), were consistent with the location of peaks in PSD (Figure 3a) and the range of

natural frequencies observed on large trees (de Langre, 2019; Moore and Maguire, 2004), and the c.o.v. for the natural frequencies indicated an accurate estimate. Consistent with experimental measurements of trees (Jonsson et al., 2007; Kane et al., 2014), the damping ratios were about 10% for both modes, but the identification uncertainty was about 10 times higher than the frequency estimates. Compared to natural frequency, the higher identification uncertainty for damping ratio was similar to other observations in engineering applications (Au, 2017; Brincker and Ventura, 2015).

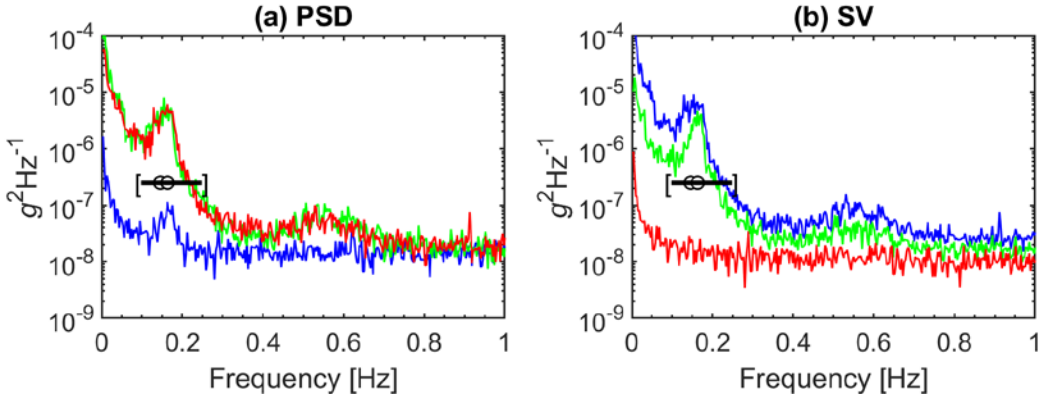

Figure 3 (a) Power spectral density (PSD) and (b) singular value (SV) spectrum (one-sided) computed from the first hour of ambient vibration recorded on a mature *Hopea odorata* Roxb. (Dipterocarpaceae) tree. In PSD plot, (blue, green, red) = (x,y,z); In SV plot, (blue, green, red) = singular value in descending order of magnitude. Note: The three lines in the SV spectrum, denoting the three eigenvalues of the real part the 3 × 3 PSD matrix at each frequency, do not correspond to the three measurement channels (x,y,z) shown in the PSD spectrum.

Since they were identified on the same band, the noise PSD for both modes were the same (Table 1), but the modal force PSD differed slightly between the two modes. The PSD of modal force (per unit modal mass) has the same unit as the PSD of the response acceleration and noise $[(\mu g)^2\ \mathrm{Hz}^{-1}]$. The modal force PSD can be used for investigating the potential dependence of modal properties on the amplitude of vibration (Section 3.4.2), and

the noise PSD can be used to verify other noise estimates. The noise PSD [17.7×10^3 $(\mu g)^2\ \mathrm{Hz}^{-1}\ = 1.77 \times 10^{-8} g^2\ \mathrm{Hz}^{-1}$] was consistent with the background noise level reflected in the SV spectrum (Figure 3b; red line). Using the formula $\gamma = S/4S_e\zeta^2$, the s/n ratio of the first and second modes was approximately 466 and 254, respectively, generally considered moderate and acceptable.

Table 1 Summary of modal properties estimated using the first hour of ambient vibration recorded on a mature *Hopea odorata* Roxb. (Dipterocarpaceae) tree.

Mode	Frequency f_i [Hz]	Damping ratio ζ_i [%]	Modal force PSD S_{ii} $[(\mu g)^2\ \mathrm{Hz}^{-1}]$	Noise PSD S_e $[(\mu g)^2\ \mathrm{Hz}^{-1}]$
1	0.128	9.8	320×10^3	17.7×10^3
	(0.76%)	(8.1%)	(6.2%)	(4.3%)
2	0.145	12	245×10^3	17.7×10^3
	(0.77%)	(7.7%)	(6.6%)	(4.3%)

Note: For each modal parameter, the first row contains the most probable value (MPV) and the second row contains the coefficient of variation (c.o.v. = standard deviation/MPV), reflecting the identification uncertainty.

Since the sensor measured translational accelerations along three orthogonal axes, the identified (partial) mode shape, $\boldsymbol{\varphi}_i$ (equation (2)), for each mode was a 3×1 vector containing the mode shape components for each DOF corresponding to a different measurement axis. The mode shape was constrained to a unit vector in three dimensions, but the length of the vectors projected onto the y-z plane was close to one for modes 1 and 2, indicating negligible vibration along the x-axis (Figure 4). Even though no such assumption was applied in the identification process, the dominant horizontal (y, z) components of the most probable mode shape for modes 1 and 2 were approximately perpendicular. Kovacic et al. (2018) similarly observed orthogonal oscillations in a leafless, unbranched tree sapling,

565 and the authors explained the vibration behavior using the mechanical properties
566 associated with the principal axes in which oscillations occurred. However, there is a need
567 for additional measurements over longer time periods to determine the prevalence of two
568 perpendicular close modes in trees and their association with tree morphometry.
569
570 Distinct from the uncertainty estimates for scalar quantities, the uncertainty for the mode
571 shape estimate, a vector-valued quantity, may not be determined by the c.o.v. of a
572 particular mode shape component corresponding to a measured DOF (Section 2.4).
573 Interpreted in a manner analogous to the c.o.v. of a scalar variate, the 'mode shape c.o.v.' is
574 defined as the square root sum of eigenvalues of the $n \times n$ posterior covariance matrix of
575 the subject $n \times 1$ mode shape vector, with n = 3 for the present case. The $n \times n$ posterior
576 covariance matrix of the mode shape can be obtained from the covariance matrix of $\boldsymbol{\theta}$
577 containing all modal parameters (Section 2.3). The mode shape c.o.v. for modes 1 and 2
578 were about 5% and 9%, respectively (Figure 4), indicating acceptable uncertainty around the
579 mode shape estimate. The mode shape uncertainty was also depicted graphically using
580 arrows spanning a four standard deviation interval (±2σ), computed using the square root of
581 the largest eigenvalue of the 3 x 3 mode shape covariance matrix, along the principal
582 direction of variation, determined using the largest eigenvector of the same matrix,
583 projected onto the y-z plane.

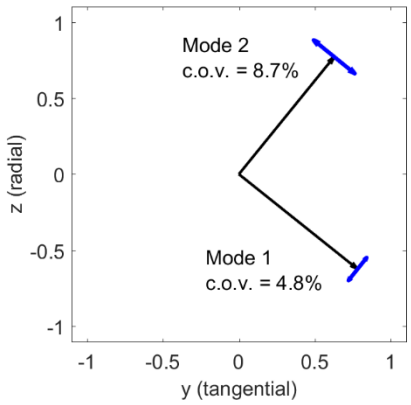

584

585 Figure 4 Most probable mode shape (black arrows) projected on the y-z plane of the sensor
586 coordinate frame and $\pm 2\sigma$ (two-sigma bound) uncertainty (blue arrows) for two close
587 modes identified using the first hour of ambient vibration recorded on a mature *Hopea*
588 *odorata* Roxb. (Dipterocarpaceae) tree.

589

590 **3.4 Analysis of long-term monitoring data**

591 Given the reasonable uncertainty for modal estimates obtained using a one-hour segment,
592 the same time window was used to examine changes in modal properties over the entire
593 week. Although some researchers have segmented longer time histories into irregular
594 intervals for analysis (Schindler and Mohr, 2018), most existing studies have used fixed
595 intervals, often one hour or less, for examining changes in the dynamic mechanical behavior
596 of trees (Granucci et al., 2013; Hale et al., 2012; Schindler et al., 2010). The choice of a time
597 window used for analysis deserves greater consideration in future work (Section 4), but the
598 one-hour segment used in this study ensured the analysis of ample FFT values in a selected
599 frequency band obtained from a time interval with reasonably consistent loading
600 conditions, precluding systematic fluctuation associated with diurnal variation or mesoscale
601 phenomena. Based on the analysis of the initial one-hour segment, the same frequency
602 band and initial guess of the natural frequencies were used consistently for all remaining
603 segments. After repeating the estimation process using consecutive, non-overlapping one-

hour segments from the one-week period of measurement, the MPVs for each modal property varied considerably over time (Figure 5). This variation may arise from environmental conditions or statistical identification error, but the change in MPVs beyond the identification error suggests the tree's modal properties varied over time. For the same periods, the modal force PSD also varied over several orders of magnitude, indicating changes in environmental conditions (e.g., wind and temperature) over the corresponding intervals. As a result of identification error, the estimates often appeared noisy, with poor continuity between consecutive data sets. In particular, the two damping ratio estimates above 20% were notably different from neighboring values, and these distinctively large values were likely associated with poor identification during periods of weak tree movement. For these two estimates, the modal force PSD was exceptionally low (< $10^{-8} g^2\ \mathrm{Hz}^{-1}$), suggesting inadequate excitation to induce vibration during the one-hour interval.

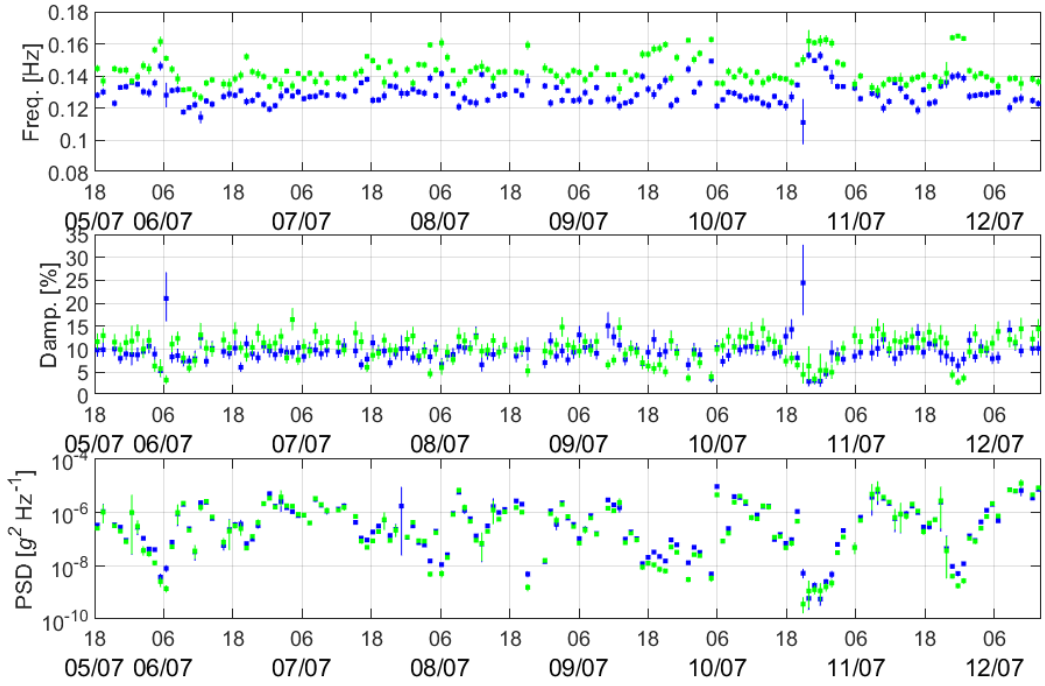

Figure 5 Tracking changes in modal properties (frequency, f_i, damping ratio, ζ_i, and modal force PSD, S_{ii}) identified from the ambient vibration of a mature *Hopea odorata* Roxb. (Dipterocarpaceae) tree over one week. Individual observations show the estimates for a one-hour time window, with a marker at the most probable value (MPV) and a $\pm 2\sigma$ error bar indicating identification uncertainty. The green and blue markers denote estimates for mode 1 and mode 2, respectively. Note: 'PSD' is the auto PSD S_{ii} of modal force.

3.4.1 Mode shape direction

Over the one-week period, the two modes occurred approximately orthogonal to one another (Figure 6). While the identified mode shape directions were generally consistent over time, the ensemble variability among one-hour intervals (~60%) was considerably greater than the identification uncertainty for a given estimate (< 10%). For modes 1 and 2, the average mode shape direction was $-37°$ (ensemble SD $21°$, c.o.v. 58%) and $46°$ (ensemble SD $29°$, c.o.v. 62%), respectively. In such cases, it is important to examine the different sources of variability carefully. While the identification uncertainty informs the

quality of the estimate, the ensemble variability often reflects changes in the modal properties or environment. A small identification uncertainty does not imply that the estimate from the next data set will be close to the current one, especially when the modal properties vary over time. For the measured tree, these observations indicate the persistent occurrence of two nearly orthogonal close modes over time.

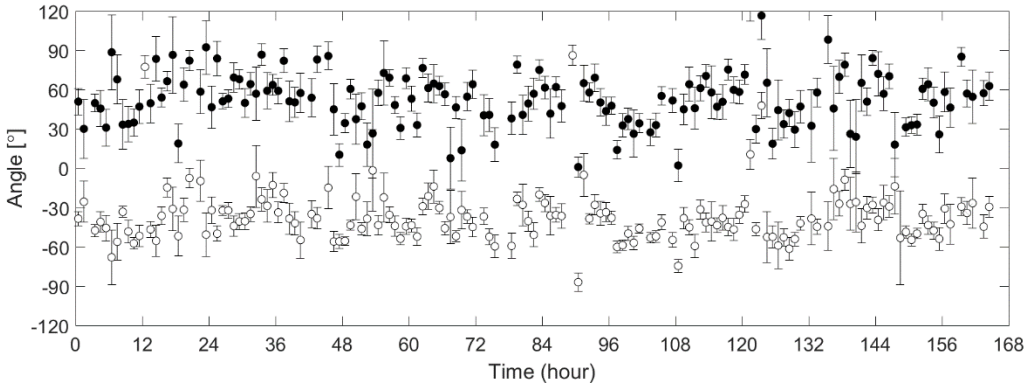

Figure 6 Tracking changes in the mode shape angle (degrees) identified from the ambient vibration of a mature *Hopea odorata* Roxb. (Dipterocarpaceae) tree over one week, with a marker at the most probably value (MPV) and a $\pm 2\sigma$ error bar indicating identification uncertainty. The empty and filled markers denote estimates for mode 1 and mode 2, respectively. Note: the mode shape angle depicts the counter-clockwise positive angle formed between the most probable mode shape and positive *y*-axis (Figure 4).

3.4.2 Potential amplitude dependence of frequency and damping ratio

After plotting modal frequency, f_i, and damping ratio, ζ_i, against the modal force PSD, S_{ii}, there was an obvious pattern among observations indicating a relationship between the modal properties and excitation intensity (Figures 7 – 8). In general, the plots showed that frequency and damping ratio varied with the excitation intensity and, consequently, vibration amplitude in opposing directions. Despite considerable scatter around the trend, the estimates indicate a strong amplitude dependence in the modal properties of trees, and the identification uncertainty for individual estimates provide a means to weigh observations in empirical models of amplitude dependence. Notably, the individual

observations depict the time-averaged dynamic behavior of trees over the time window used for analysis, and this treatment could be affected by fluctuations in environmental loads within this period. In the engineering disciplines, several researchers have attributed amplitude dependence in the vibration properties of structures (Au et al., 2012; Satake et al., 2003) to a stick-slip frictional behavior in structural components (Aquino and Tamura, 2013), possibly arising from material imperfections (Jeary, 1997), but the velocity-dependent dissipation of energy through aerodynamic drag, especially around leaves, likely contributes to the phenomenon in trees. At present, there are no clear existing reports of amplitude dependence in the modal properties of trees, and the development of empirical models from more extensive observations could illuminate this relationship, especially to supplement limited theoretical models for damping ratio. Although wind conditions were not measured in this work, it would be useful to compare the modal force PSD with suitable measurements of wind conditions near trees monitored in future work.

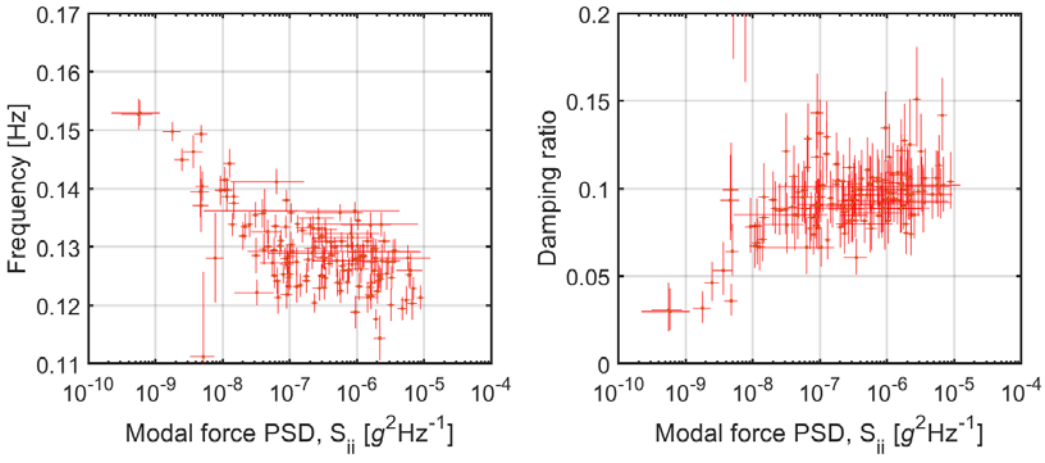

Figure 7 Scatter plot of modal frequency, f_i, and damping ratio, ζ_i, against modal force PSD, S_{ii}, for mode 1 identified from the ambient vibration of a mature *Hopea odorata* Roxb. (Dipterocarpaceae) tree over one week (two outliers with damping ratios beyond 20% are out of scale). The error bars show the $\pm 2\sigma$ identification uncertainty for each quantity.

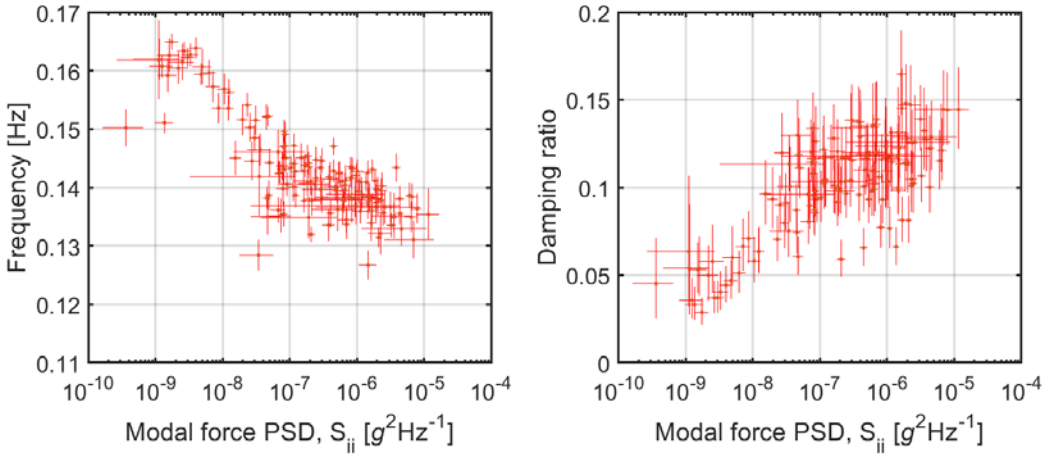

Figure 8 Scatter plot of modal frequency, f_i, and damping ratio, ζ_i, against modal force PSD, S_{ii}, for mode 2 identified from the ambient vibration of a mature *Hopea odorata* Roxb. (Dipterocarpaceae) tree over one week. The error bars show the ±2σ identification uncertainty for each quantity.

4 Challenges and practical considerations for the ambient modal identification of trees

The modal properties estimated using the Bayesian method outlined in this work were physically reasonable and consistent with existing measurements of the vibration properties of trees in the published literature (de Langre, 2019; Moore and Maguire, 2004), including other tropical broadleaf trees (Burcham et al., 2020), but it will be important to carefully consider several issues in any future work. Among all considerations, the quality and quantity of data will fundamentally influence the identification results and subsequent investigations. The noise level ($10^{-8} g^2\ \mathrm{Hz}^{-1}$) associated with the MEMS accelerometer used in this study was comparable to other commercial models, and the modal s/n ratio, in terms of PSD, varied acceptably between the low multiples of 10^1 and 10^2. Although some piezoelectric and servo accelerometers offer greater sensitivity and lower noise, especially at lower frequencies, they are often more costly, heightening risks associated with outdoor use, and require a larger power supply that constrains installation on a tree. Moreover, the

low frequency drift of data due to temperature variation and aging of electronic components, a common issue for many sensors, did not cause any obvious artefacts, since it occurred at different time scales than the dynamics of the subject mode. Still, there is a need to evaluate sensor characteristics (i.e., measurement performance, data storage, power supply, environmental protection) and assess their suitability for monitoring ambient tree vibration over long periods.

In ambient modal identification, the unknown, varying excitation force, mainly wind loads, and sensor characteristics will affect the modal s/n ratio, and it is inevitable that some modes may not be reliably identified (i.e., subject to large uncertainty) or even detected in a particular time window. Using long-term monitoring data, some of the modes may only be adequately excited intermittently to permit reliable identification by the Bayesian (or any other) algorithm. As the magnitude of wind loads and modal participation (related to the spatial correlation of wind distribution and mode shape) typically decrease with frequency, the first few modes of trees will likely be identified more consistently and accurately than higher modes.

In general, the length of the time window used for analysis should balance the conflicting requirements to maximize identification precision (the longer the better) and modeling error risk (the shorter the better), and the recently developed explicit formulas for identification uncertainty (Section 2.5) can be used to select a time window that achieves a desired level of accuracy for a particular situation. For data with acceptable s/n ratio (e.g., > 100), the required time window for a well-separated mode typically ranges from a few hundred to a thousand times the natural period, possibly extending up to nearly two hours

for large, mature trees. For close modes, the time window must be longer, depending on the proximity of modes (the closer the longer) and the coherence of modal forces (the higher the longer). Beyond these requirements, the time window should be as short as possible to reduce potential modeling error arising from non-stationary data and time-varying modal properties. If the close modes detected in this study are commonly encountered in trees, it will be important to carefully evaluate these trade-offs and recommend suitable values in future work. Especially for amplitude dependence studies requiring a range of loading conditions, the interval at which the environmental loads fluctuate should be considered alongside the requirements for identification precision to select the time window used for analysis. For example, it would be important to select the longest possible time window containing relatively consistent momentum exchange regimes when examining amplitude dependence associated with low frequency wind gusts.

5 Conclusions

Despite a longstanding interest in the vibration of trees under natural wind loading (Baker, 1997; Gardiner, 1994; Holbo, 1980; Mayer, 1987), the development of methods to identify the modal properties of trees has received relatively little attention from forest scientists. In related studies, many researchers depicted the vibration behavior of trees using representative Fourier spectra (James et al., 2006; Schindler et al., 2013b), and this descriptive approach mostly emphasized the dominant frequencies observed under certain conditions, precluding a quantitative, statistical treatment of all modal properties over time. In contrast, the method outlined in this study usefully estimates the modal properties of trees and characterizes the associated identification uncertainty. The advancement of similar methods will expand investigative opportunities for scientists interested in the

743 dynamic mechanical behavior of trees, especially to mitigate the risk of wind damage to
744 trees and forests, and it will be important to improve on existing work by examining the
745 suitability of underlying modeling assumptions and improving the numerical performance of
746 algorithms, especially for studying tree vibration during ambient wind loads. Given the
747 similarity between measurements in this study and existing reports, the method appears
748 broadly suitable for identifying the modal properties of trees in scientific and practical
749 settings. Alongside a valuable treatment of uncertainty, the measurements yielded new
750 information about the vibration behavior of large trees, including the persistent occurrence
751 of two nearly orthogonal close modes near the tree's fundamental frequency and a strong
752 amplitude dependence in frequency and damping ratio.
753

754 **6 Acknowledgement**

755 The second author was supported by grant SUG/4 (C120032000) from the Nanyang
756 Technological University, Singapore.
757

758 **7 Supplementary data**

759 The field data used in this study was deposited in the Harvard Dataverse at
760 https://doi.org/10.7910/DVN/FHJBYG. The MATLAB codes for implementing the Bayesian
761 algorithm used in this study may be obtained by contacting bayoma2ask@gmail.com.
762

8 References

Ameri, N., Grappasonni, C., Coppotelli, G., Ewins, D.J., 2013. Ground vibration tests of a helicopter structure using OMA techniques. Mech. Syst. Signal Process. 35, 35–51.

Aquino, R.E.R., Tamura, Y., 2013. On stick-slip phenomenon as primary mechanism behind structural damping in wind-resistant design applications. J. Wind Eng. Ind. Aerodyn. 115, 121–136.

Au, S.K., 2017. Operational Modal Analysis: Modeling, Bayesian Inference, Uncertainty Laws, 1st ed. Springer Nature, Singapore.

Au, S.K., 2012. Fast Bayesian ambient modal identification in the frequency domain, Part I: Posterior most probable value. Mech. Syst. Signal Process. 26, 60–75.

Au, S.K., 2011. Fast Bayesian FFT method for ambient modal identification with separated modes. J. Eng. Mech. 137, 214–226.

Au, S.K., Brownjohn, J.M.W., Li, B., Raby, A., 2021. Understanding and managing identification uncertainty of close modes in operational modal analysis. Mech. Syst. Signal Process. 147, 107018.

Au, S.K., Brownjohn, J.M.W., Mottershead, J.E., 2018. Quantifying and managing uncertainty in operational modal analysis. Mech. Syst. Signal Process. 102, 139–157.

Au, S.K., Zhang, F.L., 2011. On assessing the posterior mode shape uncertainty in ambient modal identification. Probabilistic Eng. Mech. 26, 427–434.

Au, S.K., Zhang, F.L., To, P., 2012. Field observations on modal properties of two tall buildings under strong wind. J. Wind Eng. Ind. Aerodyn. 101, 12–23.

Baker, C.J., 1997. Measurements of the natural frequencies of trees. J. Exp. Bot. 48, 1125–1132.

Brillinger, D.R., 2001. Time Series: Data Analysis and Theory, Classics in Applied Mathematics. Society for Industrial and Applied Mathematics, Philadelphia, PA.

Brincker, R., Ventura, C., 2015. Introduction to Operational Modal Analysis. Wiley.

Brincker, R., Zhang, L., Andersen, P., 2001. Modal identification of output-only systems using frequency domain decomposition. Smart Mater. Struct. 10, 441–445.

Brownjohn, J.M.W., De Stefano, A., Xu, Y.L., Wenzel, H., Aktan, A.E., 2011. Vibration-based monitoring of civil infrastructure: Challenges and successes. J. Civ. Struct. Health Monit. 1, 79–95.

Bruchert, F., Gardiner, B.A., 2006. The effect of wind exposure on the tree aerial architecture and biomechanics of Sitka spruce (*Picea sitchensis*, Pinaceae). Am. J. Bot. 93, 1512–1521.

Bunce, A., Volin, J.C., Miller, D.R., Parent, J., Rudnicki, M., 2019. Determinants of tree sway frequency in temperate deciduous forests of the Northeast United States. Agric. For. Meteorol. 266–267, 87–96.

Burcham, D.C., Autio, W.R., James, K., Modarres-Sadeghi, Y., Kane, B., 2020. Effect of pruning type and severity on vibration properties and mass of Senegal mahogany (*Khaya senegalensis*) and rain tree (*Samanea saman*). Trees Struct. Funct. 34, 213–228. https://doi.org/10.1007/s00468-019-01912-8

Burgess, A.J., Retkute, R., Preston, S.P., Jenson, O.E., Pound, M.E., Pridmore, T.P., Murchie, E.H., 2016. The 4-dimensional plant: Effects of wind-induced canopy movement on light fluctuations and photosynthesis. Front. Plant Sci. 7, 1392.

Castro-Garcia, S., Blanco-Roldan, G.L., Gil-Ribes, J.A., Aguera-Vega, J., 2008. Dynamic analysis of olive trees in intensive orchards under forced vibration. Trees Struct. Funct. 22, 795–802.
Caughey, T.K., O'Kelly, M.E.J., 1965. Classical normal modes in damped linear dynamic systems. J. Appl. Mech. 32, 583–588.
Ciruzzi, D.M., Loheide, S.P., 2019. Monitoring tree sway as an indicator of water stress. Geophys. Res. Lett. 46, 21–29.
Cooley, J.W., Tukey, J.W., 1965. An algorithm for the machine calculation of the complex Fourier series. Math. Comput. 19, 297–301.
Daniel, T.L., 1984. Unsteady aspects of aquatic locomotion. Am. Zool. 24, 121–134.
de Langre, E., 2019. Plant vibrations at all scales: A review. J. Exp. Bot. 70, 3521–3531. https://doi.org/10.1093/jxb/erz209
DeVivo, A., Brutti, C., Leofanti, J.L., 2013. Modal shape identification of a large structure exposed to excitation by operational modal analysis technique. Mech. Syst. Signal Process. 32, 195–206.
Gardiner, B.A., 1995. The interactions of wind and tree movement in forest canopies, in: Coutts, M.P., Grace, J. (Eds.), Wind and Trees. University of Cambridge, Cambridge, UK, pp. 41–59.
Gardiner, B.A., 1994. Wind and wind forces in a plantation spruce forest. Bound.-Layer Meteorol. 67, 161–186.
Gardiner, B.A., 1989. Mechanical characteristics of Sitka spruce (No. Occasional Paper 24). Forestry Commission, Edinburgh, United Kingdom.
Gougherty, A.V., Keller, S.R., Kruger, A., Stylinski, C.D., Elmore, A.J., Fitzpatrick, M.C., 2018. Estimating tree phenology from high frequency tree movement data. Agric. For. Meteorol. 263, 217–224.
Granucci, D., Rudnicki, M., Hiscox, A., Miller, D., Su, H.B., 2013. Quantifying the effects of freezing on tree sway frequencies. Agric. For. Meteorol. 168, 10–14.
Hale, S.E., Gardiner, B.A., Wellpott, A., Nicoll, B.C., Achim, A., 2012. Wind loading of trees: Influence of tree size and competition. Eur. J. For. Res. 131, 203–217.
Holbo, R., 1980. Aeromechanical behavior of selected Douglas-fir. Agric. Meteorol. 21, 81–91.
Jackson, T., Shenkin, A., Moore, J., Bunce, A., van Emmerik, T., Kane, B., Burcham, D.C., James, K., Selker, J., Calders, K., Origo, N., Disney, M., Burt, A., Wilkes, P., Raumonen, P., Gonzalez de Tanago Menaca, J., Lau, A., Herold, M., Goodman, R.C., Fourcaud, T., Malhi, Y., 2019. An architectural understanding of natural sway frequencies in trees. J. R. Soc. Interface 16, 1–9.
James, K.R., Haritos, N., Ades, P.K., 2006. Mechanical stability of trees under dynamic loads. Am. J. Bot. 93, 1522–1530.
Jeary, A.P., 1997. Damping in structures. J. Wind Eng. Ind. Aerodyn. 72, 345–355.
Jonsson, M.J., Foetzki, A., Kalberer, M., Lundstrom, T., Ammann, W., Stockli, V., 2007. Natural frequencies and damping ratios of Norway spruce (*Picea abies* (L.) Karst) growing on subalpine forested slopes. Trees Struct. Funct. 21, 541–548.
Kane, B., 2018. The effect of simulated trunk splits, pruning, and cabling on sways of *Quercus rubra* L. Trees Struct. Funct. 32, 985–1000. https://doi.org/10.1007/s00468-018-1690-3
Kane, B., Modarres-Sadeghi, Y., James, K.R., Reiland, M., 2014. Effects of crown structure on the sway characteristics of large decurrent trees. Trees Struct. Funct. 28, 151–159.

Kooreman, B., 2013. Measuring weight fluctuations in trees based on natural frequency (Master's Thesis). Delft University of Technology, Delft, Netherlands.
Kovacic, I., Radomirovic, D., Zukovic, M., Pavel, B., Nikolic, M., 2018. Characterisation of tree vibrations based on the model of orthogonal oscillations. Sci. Rep. 8, 1–11.
Li, B., Au, S.K., 2019. An expectation-maximization algorithm for Bayesian operational modal analysis with multiple (possibly close) modes. Mech. Syst. Signal Process. 132, 490–511.
Mayer, H., 1987. Wind-induced tree sways. Trees Struct. Funct. 1, 195–206.
Miesbauer, J.W., Gilman, E.F., Giurcanu, M., 2014. Effects of tree crown structure on dynamic properties of *Acer rubrum* L. 'Florida Flame'™. Arboric. Urban For. 40, 218–229.
Milne, R., 1991. Dynamics of swaying *Picea sitchensis*. Tree Physiol. 9, 383–399.
Moore, J.R., Maguire, D.A., 2004. Natural sway frequencies and damping ratios of trees: Concepts, review and synthesis of previous studies. Trees Struct. Funct. 18, 195–203.
Peeters, B., De Roeck, G., 2001. Stochastic System Identification for Operational Modal Analysis: A Review. J. Dyn. Syst. Meas. Control 123, 659–667.
Pintelon, R., Schoukens, J., 2001. System Identification: A Frequency Domain Approach, 1st ed. Wiley-IEEE Press.
Reiland, M., Kane, B., Modarres-Sadeghi, Y., Ryan, H.D.P., 2015. The effect of cables and leaves on the dynamic properties of red oak (*Quercus rubra*) with co-dominant stems. Urban For. Urban Green. 14, 844–850.
Roden, J., Pearcy, R., 1993. Photosynthetic gas exchange response of poplars to steady-state and dynamic light environments. Oecologia 93, 208–214.
Satake, N., Suda, K., Arawaka, T., Sasaki, A., Tamura, A., 2003. Damping evaluation using full-scale data of buildings in Japan. J. Struct. Eng. 129, 470–477.
Scannell, B., 1983. Quantifications of the interactive motions of the atmospheric surface layer and a conifer canopy (PhD Thesis).
Schindler, D., Fugmann, H., Mayer, H., 2013a. Analysis and simulation of dynamic response behavior of Scots pine trees to wind loading. Int. J. Biometeorol. 57, 819–833.
Schindler, D., Fugmann, H., Schonborn, J., Mayer, H., 2012. Coherent response of a group of plantation-grown Scots pine trees to wind loading. Eur. J. For. Res. 131, 191–202.
Schindler, D., Mohr, M., 2019. No resonant response of Scots pine trees to wind excitation. Agric. For. Meteorol. 265, 227–244.
Schindler, D., Mohr, M., 2018. Non-oscillatory response to wind loading dominates movement of Scots pine trees. Agric. For. Meteorol. 250–251, 209–216.
Schindler, D., Schonborn, J., Fugmann, H., Mayer, H., 2013b. Responses of an individual deciduous broadleaved tree to wind excitation. Agric. For. Meteorol. 177, 69–82.
Schindler, D., Vogt, R., Fugmann, H., Rodriguez, M., Schonborn, J., Mayer, H., 2010. Vibration behavior of plantation-grown Scots pine trees in response to wind excitation. Agric. For. Meteorol. 150, 984–993.
Schipfors, M., Fabbrocino, G., 2014. Operational modal analysis of civil engineering structures: An introduction and guide for applications, 1st ed. Springer-Verlag, New York, NY.
Sellier, D., Fourcaud, T., 2005. A mechanical analysis of the relationship between free oscillations of *Pinus pinaster* Ait. saplings and their aerial architecture. J. Exp. Bot. 56, 1563–1573.

Sellier, D., Suzuki, S., 2020. Age dynamics of wind risk and tree sway characteristics in a softwood plantation. Front. For. Glob. Change 3, 89.
Shih, C.Y., Tsuei, G., Allemang, R.J., Brown, D.L., 1988. Complex mode indication function and its applications to spatial domain parameter estimation. Mech. Syst. Signal Process. 2, 367–377.
Spatz, H.C., Theckes, B., 2013. Oscillation damping in trees. Plant Sci. 207, 66–71.
Stull, R.B., 1988. An Introduction to Boundary Layer Meteorology. Kluwer Academic Publishing, Boston, MA.
van Emmerik, T., Steele-Dunne, S., Gentine, P., Oliveira, R.S., Bittencourt, P., Barros, F., van de Giesen, N., 2018. Ideas and perspectives: Tree-atmosphere interaction responds to water-related stem variations. Biogeosciences 15, 6439–6449.
van Emmerik, T., Steele-Dunne, S., Hut, R., Gentine, P., Guerin, M., Oliveira, R.S., Wagner, J., Selker, J., Giesen, N. van de, 2017. Measuring tree properties and responses using low-cost accelerometers. Sensors 17, 1–17.
van Overschee, P., de Moor, B.L., 1996. Subspace Identification for Linear Systems: Theory - Implementation - Applications, 1st ed. Springer US.
Vogel, S., 2009. Leaves in the lowest and highest winds: Temperature, force and shape. New Phytol. 183, 13–26.
Vollsinger, S., Mitchell, S.J., Byrne, K.E., Novak, M.D., Rudnicki, M., 2005. Wind tunnel measurements of crown streamlining and drag relationships for several hardwood species. Can. J. For. Res. 35, 1238–1249.
Yuen, K.V., Katafygiotis, L.S., 2003. Bayesian fast Fourier transform approach for modal updating using ambient data. Adv. Struct. Eng. 6, 81–95.
Zhu, Z., Au, S.K., Li, B., Xie, Y.L., 2021. Bayesian operational modal analysis with multiple setups and multiple (possibly close) modes. Mech. Syst. Signal Process. 150, 107261.

Appendix I. Nomenclature

	Abbreviations
DOF(s)	Degree(s) of freedom
FT, FFT	Fourier Transform, Fast Fourier Transform
PSD	Power spectral density
SV	Singular value
NLLF	Negative log-likelihood function
MPV	Most probable value
OMA	Operational modal analysis
	Basic symbols
$\boldsymbol{i}$	Purely imaginary number; $\boldsymbol{i} = \sqrt{-1}$
$\boldsymbol{I}_n$	$n \times n$ identity matrix
t	Time (s)
Δt	Time interval (s)
N	Number of samples in a time window of data used for modal identification
f_k	FFT frequency (Hz)
	Structural dynamics
$\boldsymbol{X}(t)$	Displacement (m) vector for all DOFs in the equation of motion
$\dot{\boldsymbol{X}}(t)$	Velocity ($\mathrm{m\ s^{-1}}$) vector for all DOFs in the equation of motion
$\ddot{\boldsymbol{X}}(t)$	Acceleration ($\mathrm{m\ s^{-2}}$) vector for all DOFs in the equation of motion
$\boldsymbol{M}$	Mass (kg) matrix
$\boldsymbol{C}$	Damping [$\mathrm{N\ m^{-1}\ s^{-1}}$] matrix
$\boldsymbol{K}$	Stiffness ($\mathrm{N\ m^{-1}}$) matrix
$\boldsymbol{F}(t)$	Time-varying force (N) vector
	Modal dynamics
f_i	Natural frequency (Hz) of mode i
ω_i	Natural frequency ($\mathrm{rad\ s^{-1}}$) of mode i; $\omega_i = 2\pi f_i$
ζ_i	Damping ratio (dimensionless) of mode i
$\boldsymbol{\psi}_i$	Mode shape (dimensionless column vector) of mode i
$p_i(t)$	Modal force per unit modal mass ($\mathrm{N\ kg^{-1}}$) of mode i
$\eta_i(t)$	Modal displacement of mode i
h_{ik}	Frequency response function (dimensionless) of mode i at frequency f_k
	Modal identification
n	Number of measured DOFs
m	Number of modes in a frequency band
N_f	Number of FFT points in a frequency band
$\ddot{\boldsymbol{x}}_j$	Measured acceleration (g = 9.81 $\mathrm{m\ s^{-2}}$) at time step j ($n \times 1$ vector)
$\boldsymbol{F}_k$	Scaled FFT ($g\ \mathrm{Hz^{-1/2}}$) of $\{\ddot{\boldsymbol{x}}_j\}_{j=0}^{N-1}$ at frequency f_k ($n \times 1$ vector)
$\boldsymbol{\varphi}_i$	Mode shape (dimensionless) confined to the measured DOFs ($n \times 1$ vector)
$\boldsymbol{\varepsilon}(t_j)$	Sensor noise (g) at time t_j ($n \times 1$ vector)
$\boldsymbol{\varepsilon}_k$	Scaled FFT ($g\ \mathrm{Hz^{-1/2}}$) of sensor noise at frequency f_k
S_{ij}	Cross-PSD ($g^2\ \mathrm{Hz^{-1}}$) between p_i and p_j

S_e	PSD ($g^2\ \mathrm{Hz}^{-1}$) of sensor noise
$\boldsymbol{E}_k$	Theoretical $n \times n$ PSD matrix of measured data
$\boldsymbol{\theta}$	Vector of modal properties
$L(\{\boldsymbol{F}_k\}, \boldsymbol{\theta})$	Likelihood function with FFT $\{\boldsymbol{F}_k\}$ data evaluated at $\boldsymbol{\theta}$

927